Lellouch et al. *EPJ Quantum Technology* (2023) 10:9
https://doi.org/10.1140/epjqt/s40507-023-00165-2

EPJ Quantum Technology
a SpringerOpen Journal

RESEARCH Open Access

Polychromatic atom optics for atom interferometry

Samuel Lellouch[1], Oliver Ennis[1], Ramiz Haditalab[1], Mehdi Langlois[1] and Michael Holynski[1*]

*Correspondence:
m.holynski@bham.ac.uk
[1]School of Physics and Astronomy, University of Birmingham, B15 2TT Edgbaston, UK

Abstract

Coherent manipulation of atoms with atom-optic light pulses is central to atom interferometry. Achieving high pulse efficiency is essential for enhancing fringe contrast and sensitivity, in particular for large-momentum transfer interferometers which use an increased number of pulses. We perform an investigation of optimizing the frequency domain of pulses by using tailored polychromatic light fields, and demonstrate the possibility to deliver high-efficiency and resilient atom-optic pulses even in the situation of inhomogeneous atomic clouds and laser beams. We find that this approach is able to operate over long interrogation times despite spontaneous emission and to achieve experimentally relevant pulse efficiencies for clouds up to 100 μK. This overcomes some of the most stringent barriers for large-momentum transfer and has the potential to reduce the complexity of atom interferometers. We show that polychromatic light pulses could enhance single-photon-based large-momentum transfer atom interferometry—achieving 850 $\hbar k$ of momentum splitting with experimentally accessible parameters, which represents a significant improvement over the state-of-the art. The benefits of the method extend beyond atom interferometry and could enable groundbreaking advances in quantum state manipulation.

Keywords: Atom-optics; Atom interferometry; Large momentum transfer

1 Introduction

Many quantum technologies rely on the coherent manipulation of atomic states. In atom interferometry-based quantum sensors, splitting and recombining atomic wavepackets [1–3] is achieved through suitable light pulses delivering a specific fraction of population transfer [4]. Fringe contrast and sensor sensitivity are ultimately bounded by the efficiency of these elementary operations. Those are however reduced in practice by inhomogeneities experienced by the atomic wavepacket [5–7] and sources of decoherence. As different atoms within the cloud experience different laser intensities (due to their positions within the beam) and see different Doppler-shifted laser frequencies (due to their individual thermal velocities), common pulses fail to simultaneously address all of them, resulting in a reduced overall pulse efficiency. Additionally, spontaneous emission causes decoherence leading to atom losses also reducing the pulse efficiency. These effects become especially limiting in large-momentum transfer (LMT) atom interferometry [8–15]

where high pulse efficiency must be maintained over long pulse sequences despite cloud expansion, accumulated Doppler shifts and spontaneous emission. Current efforts to deliver more homogeneous beams remain limited by the available technology. Interesting approaches like composite pulses [5, 16–18]—where the phase of the beams is tuned to increase pulse resilience—and adiabatic passages [19, 20] have been developed, as well as recent demonstrations including driving an interferometer using frequency combs [21] and the use of Floquet atom optics [22]. However, most of these typically require longer pulse durations, leading to more decoherence from spontaneous emission, which remains a limiting factor in single-photon LMT atom interferometry [11] yet to be addressed by any scheme.

In this article, we take a different approach by proposing to optimize the frequency domain of pulses, and implement it to drive atom optic transitions using polychromatic light pulses. While most existing literature relies on the paradigmatic monochromatic pulse model [23], studies have pointed out the richer internal dynamics of an atom subjected to light fields comprised of several frequencies [24–27]. With a plethora of exotic effects [28–31], they offer additional handles to control and optimize the atom-light dynamics. In this work, we demonstrate the ability to tailor such fields to increase the pulse resilience to atomic cloud inhomogeneity, hence delivering high-efficiency pulses at the atomic cloud scale [see Fig. 1]. Moreover, by tailoring the light fields to design non-trivial atomic internal dynamics, we demonstrate a reduced impact of spontaneous emission in single photon interferometers over unprecedented times. We find that such schemes can enable major benefits for LMT atom interferometry with currently available technology.

2 Results

Polychromatic dynamics Consider a two-level atom ($|g\rangle, |e\rangle$) as used in single-photon[1] atom interferometry [32],[2] driven by a generic structured polychromatic field containing $\mathcal{N}$ frequency components at frequencies $\omega_n = \omega_L + \delta\omega_n$, where we have introduced ω_L as the central laser frequency. Here, we consider a regime where the frequency differences $\delta\omega_n$ are at the scale of the Rabi frequency (≈kHz–MHz), hence much smaller than the optical frequencies ω_n, ω_L. In this regime, using the rotating wave approximation permits to neglect fast-oscillating terms at optical frequencies so that the coherent atom dynamics take the general form

$$i\partial_t \begin{pmatrix} c_g \\ c_e \end{pmatrix} = \begin{pmatrix} 0 & \Omega(t)/2 \\ \Omega^*(t)/2 & \Delta \end{pmatrix} \begin{pmatrix} c_g \\ c_e \end{pmatrix}, \tag{1}$$

with $\Omega(t) = \sum_n \Omega_n e^{i(\delta\omega_n t + \phi_n)}$ where Ω_n is the individual Rabi frequency of the nth frequency component,[3] ϕ_n its phase, and $\Delta \equiv \omega_{at} - \omega_L$ with ω_{at} the atomic frequency. The coefficients $c_e(t)$, $c_g(t)$ are the excited—and ground-state wavefunction amplitudes and

[1] We anticipate that the ideas presented here could be adapted to the case of two-photon transitions such as Bragg or Raman schemes, which reduce to an effective single-photon problem under suitable conditions, although a proper derivation would require a careful treatment.

[2] In an atom interferometer where internal and momentum degrees of freedom are entangled, the two quantum states live in a tensorial product of the two (internal and momentum) Hilbert spaces. Here, as the difference in momentum imparted by the different field components remains extremely small, $|\mathbf{k_n} - \mathbf{k_m}| \ll \mathbf{k_L}$, we can safely assume that the system can still be considered as a two-level system.

[3] Equation (1) generically describes any linear interaction between a two-level atom and an electric field, yet the exact relation between Ω_n and the electric field amplitude of the n-th component depends on the considered transition.

fulfill the normalization condition $|c_e|^2 + |c_g|^2 = 1$. In the presence of spontaneous emission, the dynamics are captured instead by the optical Bloch equations (OBE) on the density operator $\hat{\rho}$

$$\begin{aligned} i\partial_t \rho_{eg} &= -\left(i\frac{\Gamma}{2} + \Delta\right)\rho_{eg} - \Omega(t)\left(\rho_{ee} - \frac{1}{2}\right), \\ i\partial_t \rho_{ee} &= -i\Gamma\rho_{ee} - 2i\,\mathrm{Im}\big[\Omega(t)\rho_{eg}\big] \end{aligned} \tag{2}$$

with Γ^{-1} the lifetime of the excited state.

When considering an atomic cloud, we introduce the cloud-averaged transition probability defined as

$$\big\langle P_{g\to e}(t)\big\rangle = \int_{\mathbf{v}}\int_{\mathbf{r}} f(\mathbf{r}) f_v(\mathbf{v}) P_{g\to e}[t,\mathbf{r},\mathbf{v}]\, d^3\mathbf{v}\, d^3\mathbf{r}, \tag{3}$$

where $f(\mathbf{r})$ is the cloud spatial distribution, $f_v(\mathbf{v})$ its velocity distribution, and $P_{g\to e}[t,\mathbf{r},\mathbf{v}]$ is the excited state probability of a single atom at position $\mathbf{r}$ and velocity $\mathbf{v}$ initially in the ground-state, after a pulse duration t. This single-atom probability is given by $|c_e|^2 = \rho_{ee}$, which can be numerically computed by solving Eqs. (1)–(2) with initial condition $\rho_{gg}(0) = |c_g(0)|^2 = 1$ and substitutions $\Delta \to \Delta - \mathbf{k_L}.\mathbf{v}$ (Doppler shift on each frequency of the driving field[4]) and $\Omega_n \to \Omega_{n,\mathbf{r}}$ (with $\Omega_{n,\mathbf{r}}$ encoding the spatial dependence of the Rabi frequency of each component of the driving field). In all this work, we will assume a Maxwell–Boltzman velocity distribution, $f_v(\mathbf{v}) = \frac{1}{(2\pi)^{3/2}\sigma_v^3}\exp^{-\mathbf{v}^2/2\sigma_v^2}$ with $\sigma_v = \sqrt{k_B T/m}$, and a Gaussian spatial distribution for the cloud, $f(\mathbf{r}) = \frac{1}{(2\pi)^{3/2}\sigma_{\mathrm{pos}}^3}\exp^{-\mathbf{r}^2/2\sigma_{\mathrm{pos}}^2}$.

In polychromatic fields, the interplay between the different frequency components in $\Omega(t)$ generically gives rise to time-dependent interference effects underlying a non-trivial dynamics in Eqs. (1)–(2) [see Sect. A.1 in the Appendix]. In particular, at variance with monochromatic Rabi oscillations, polychromatic dynamics generally show an asymmetry in the occupation of the ground and excited states, as observed in a variety of situations at the single-atom level [24–27, 31] and depicted on Fig. 1. However, extending to many-atom clouds results in averaging and incoherence, possibly blurring out these effects. For usual monochromatic pulses, this results in a loss of contrast and damping of Rabi oscillations [see Fig. 1]. In the following, we demonstrate that through a suitable tailoring of polychromatic fields, such features can be preserved and further exploited to achieve disruptive pulse efficiency, resilience and coherence.

Tailored polychromatic fields We consider polychromatic models with the form of frequency combs, which offer an intuitive framework while being versatile to experimentally implement and tailor. We assume a comb of frequencies centred around the laser frequency ω_L and made of N evenly-spaced pairs of symmetrically-detuned peaks. Denoting $\delta\omega$ as the spacing between adjacent peaks, we will consider two situations: (i) Spectra with a resonant component, in which case the field has components at frequencies $\delta\omega_n = n\delta\omega$, $n \in \mathbb{Z}$; (ii) Spectra with no resonant component, in which case the field has components at frequencies $\delta\omega_n = (n - \mathrm{sign}(n)/2)\delta\omega$, $n \in \mathbb{Z}^*$ [see Fig. 2]. We assume the polychromatic light

[4] As the spectrum wavevector dispersion remains extremely small, $|\mathbf{k_n} - \mathbf{k_m}| \ll \mathbf{k_L}$, we find that assuming a global Doppler shift of $\mathbf{k_L}.\mathbf{v}$ for all frequencies is a very accurate approximation here.

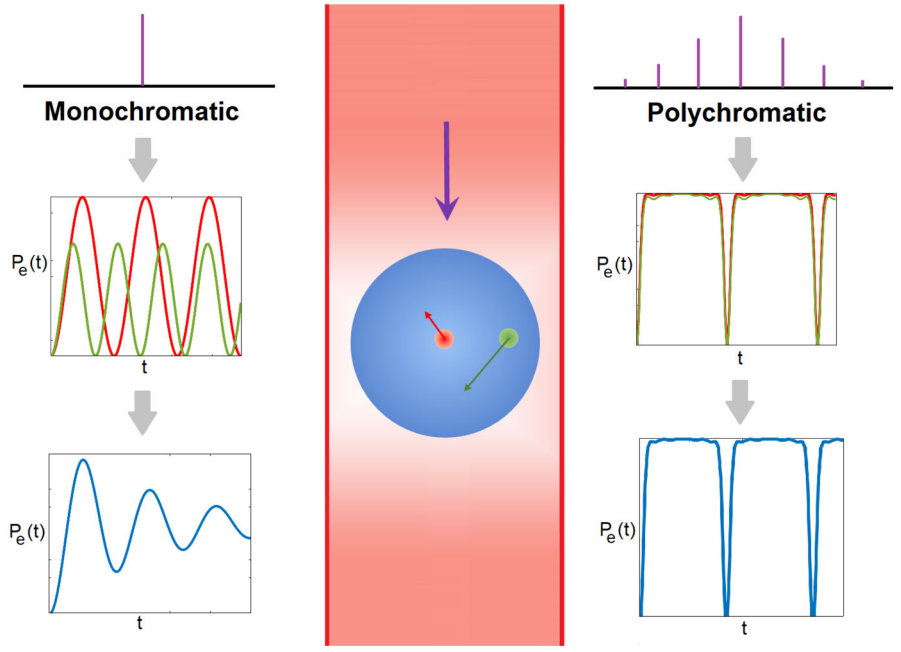

Figure 1 Illustrative comparison between the monochromatic and polychromatic dynamics of different atoms within a cloud, and the resulting cloud-average. This drawing is based on simulation results obtained with a polychromatic comb of type C [see Fig. 2] with $\alpha = 0.9$; the representation of the spectra above is purely illustrative though

to be aligned along the z-axis, and create a Gaussian spatial intensity distribution in the (x, y) plane, $I(\mathbf{r}) = I_0 \exp^{-(x^2+y^2)/2\sigma^2_{\text{beam}}}$. Introducing the Rabi frequency associated with the total intensity at the center of the beam, $\Omega_T = d/\hbar\sqrt{2I_0/c\epsilon_0}$,[5] individual Rabi frequencies $\Omega_{n,\mathbf{r}}$ therefore read[6] $\Omega_{n,\mathbf{r}} = \Omega_n \exp^{-(x^2+y^2)/4\sigma^2_{\text{beam}}}$ with the power normalisation condition $\sum_n {\Omega_n}^2 = \Omega_T^2$. We assume here a constant power ratio α between two adjacent pairs of peaks, $\alpha = {\Omega_{n+1}}^2/{\Omega_n}^2$ for all $n \geq 0$. In the particular case $\alpha = 1$ (equal amplitude comb), it gives $\Omega_n = \Omega_T/\sqrt{\mathcal{N}}$ where $\mathcal{N} = 2N + 1$ is the number of peaks with a resonant component, and $\mathcal{N} = 2N$ without. We further introduce the comb aspect ratio $\epsilon \equiv \delta\omega/\Omega_{n_0}$ with Ω_{n_0} the Rabi frequency of the most central component ($n_0 = 0, 1$ depending on whether there is a resonant component).

A detailed description of the dynamics of a single atom subjected to such frequency combs is provided in Sect. A.1 in the Appendix. In particular, we find there that two conditions enable the design of flat extended oscillation plateaus: an aspect ratio $\epsilon = 1$, and all field components to be in phase, $\phi_n = 0$; in this case, constructive time-dependent interference indeed occurs between field components as visible from Eq. (4) [Sect. A.1]. In the following, we work under these conditions and evidence how tailoring such flat asymmetric Rabi oscillations enables an increased pulse efficiency, resilience and coherence at the atomic cloud scale.

[5] This is assuming an electric-dipole interaction; the relation between Rabi frequency and intensity may be different for other types of transitions.

[6] This assumes the same intensity distribution for all field components.

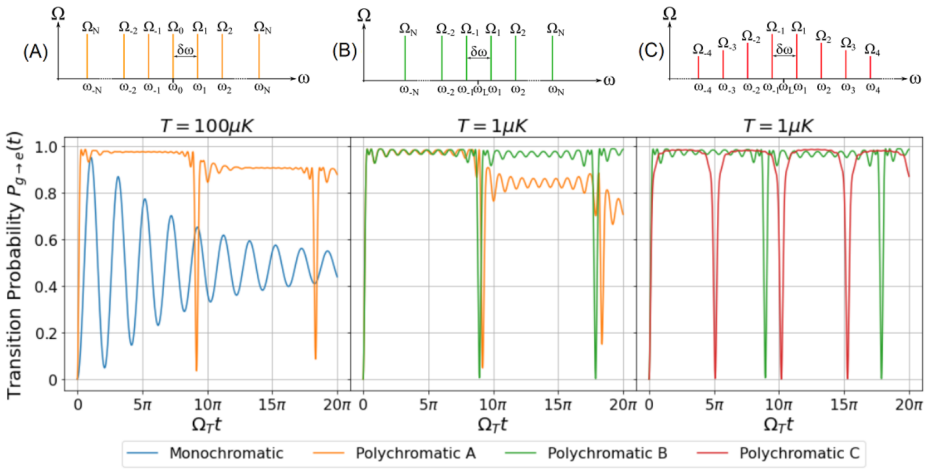

Figure 2 Cloud-averaged transition probability without considering spontaneous emission for a monochromatic pulse (blue) and three polychromatic spectra A, B (equal amplitude, $N = 10$) and C ($\alpha = 0.7$) with the same total Rabi frequency $\Omega_T = 4.8$MHz (which correponds for instance to a power $P = 100$ mW on the $^1S_0$–$^3P_1$ transition in ^{87}Sr). Combs B and C have no resonant component and the aspect ratio is $\epsilon = 1$ in all three cases. Here, $\sigma_{\text{pos}} = 2$ mm and $\sigma_{\text{beam}} = 5$ mm. While polychromatic fields display an enhanced efficiency even at high temperatures (left), contrast loss over time can be eliminated by removing the resonant component (middle), and smooth population transfers can be performed by shaping the pulse power spectrum (right)

Pulse efficiency and temperature resilience Figure 2 compares the cloud-averaged transition probability obtained with three polychromatic comb models and a monochromatic field of same total power and intensity distribution, in the absence of spontaneous emission. With a maximal probability transition topping ≈1, we find that polychromatic pulses permit higher-efficiency population transfers for the atomic cloud. This can be understood from an enhanced resilience to cloud averaging arising from the robustness of the scheme to individual atomic positions and velocities. On the one hand, clean plateaus reduce the sensitivity to pulse duration and local Rabi frequency inhomogeneities within the cloud.[7] Therefore, we define the polychromatic π-time as the duration to reach the middle of the first plateau. On the other hand, polychromatic combs remain rather insensitive to individual thermal Doppler shifts, which arises from the combs being regular and narrowly-spaced—ensuring any detuned atom will be near-resonant with another close peak—and from their high bandwidth: while we find here that $\epsilon \approx 1$ is enough to ensure the former, the pulse bandwidth Δ_{BW} at fixed ϵ can be increased at no cost of optical power by increasing the number of peaks, $\Delta_{\text{BW}} \propto \sqrt{\mathcal{N}}$. This guarantees high resilience to detunings and thermal averaging [see Fig. 3, left]. As a result, polychromatic pulses could enable high-efficiency quantum state manipulation at high temperatures, removing major complexity barriers in atom-optics based quantum technologies.

Comb tailoring With standard pulse shaping techniques [33–35], interesting pulse properties can be designed by tailoring the spectrum envelope. For example, introducing a power ratio $\alpha < 1$ produces smoother plateaus [Fig. 2, right], which ensures that the single-atom π-time, $\tau_\pi^{\text{poly}} = \pi/\delta\omega$ [see Sect. A.1 in the Appendix], can be used as an optimal pulse

[7] This is slightly subtler as atoms at different positions experience different aspect ratios ϵ; yet, an appropriate choice of $\epsilon = 1$ proves optimal here.

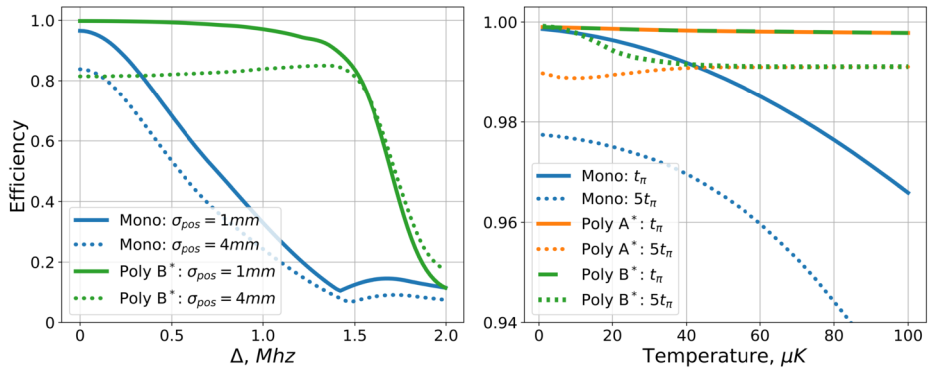

Figure 3 Left: Efficiency of a π-pulse as a function of detuning $\Delta = \omega_{at} - \omega_L$ for a monochromatic and a polychromatic [spectrum (B), $N = 10$, $\epsilon = 1$] pulse without considering spontaneous emission, with $T = 100\ \mu$K, $\Omega_T = 4.8$MHz and $\sigma_{\text{beam}} = 5$ mm. The efficiency is obtained by taking the cloud-averaged transition probability at the chosen π-time (monochromatic: first Rabi maximum; polychromatic: middle of the first plateau). Due to their larger bandwidth, polychromatic pulses are more resilient to detunings. Right: Efficiency of a π- and 5π-pulse as a function of cloud temperature in the monochromatic and two polychromatic cases [combs (A) and (B), $N = 10$, $\epsilon = 1$] with $\Omega_T = 4.8$MHz, $\sigma_{\text{pos}} = 1$ mm and $\sigma_{\text{beam}} = 5$ mm. Polychromatic pulses enable a higher efficiency up to large temperatures, which can be maintained over several Rabi cycles by removing the comb's resonant component

duration even when addressing a cloud with no reduction of the pulse efficiency—an asset over monochromatic pulses. However, polychromatic combs offer further tailoring options, especially at long timescales where the discreteness of the spectrum—and not only its envelope—starts to be relevant. An interesting effect is the mitigation of contrast loss over long pulse times. While monochromatic Rabi oscillations are unavoidably damped due to accumulating dephasings between atoms, we find that polychromatic fields with no resonant component are more robust [Fig. 2, middle]. This can be understood from Eq. (4) [Sect. A.1 in the Appendix], which shows that in the absence of a resonant component, the oscillation frequency for a given atom does not depend on the local Rabi frequency but only on $\delta\omega$ so all atoms oscillate in phase. At low temperature, when only position effects are relevant, this results in a complete suppression of the damping [Fig. 3, right]. When increasing the temperature, the Doppler broadening of the peaks makes the two models (A) and (B) more indistinguishable so that they both converge to an intermediate behaviour where the damping saturates to a stationary value after a few cycles.

Spontaneous emission mitigation Another appealing feature of polychromatic pulses is the suppression of spontaneous emission, which, in monochromatic pulses, usually introduces an unavoidable decay of the amplitude of Rabi oscillations. For instance, on the intercombination line transition $^1S_0$–$^3P_1$ on ^{87}Sr ($\lambda = 689$ nm, $\Gamma = 2\pi \times 7.4$ kHz), the excited-state lifetime of 21.6 μs is a severe limiting factor for long pulse sequences such as desired in LMT interferometry [11]. Here, we demonstrate that designing highly asymmetric dynamics within the pulse timescale can overcome this barrier by allowing the atoms to spend most of their time in the ground-state. To do so, we use here an equal-amplitude comb (B) with $\epsilon = 1$. Figure 4 displays the polychromatic dynamics of a ^{87}Sr atom initially in the ground—(red dashed line) or excited—(green solid line) state. While starting in the ground state increases spontaneous emission over the monochromatic case (blue) as a consequence of the atom spending longer time in the excited state, starting in the excited

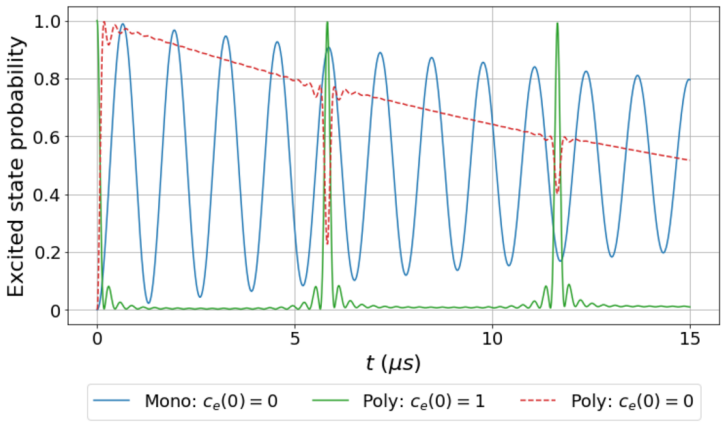

Figure 4 Single-atom monochromatic (blue) and polychromatic (red/green) dynamics of a ^{87}Sr atom on the $^1S_0$–$^3P_1$ transition for different initial conditions. Used here is comb (B) with $N = 10$ and $P = 100$ mW, $\sigma_{\text{beam}} = 5$ mm (hence $\Omega_T = 4.8$MHz). When starting the polychromatic dynamics in the ground state (red dashed), spontaneous emission is enhanced over the monochromatic case due to the atom's plateauing in the excited state. Conversely, when starting in the excited state (green), the atom spends very little time in it, resulting in reduced spontaneous emission

state strongly suppresses it, as the atom spends most of its time in the ground state. The latter approach enables the maintenance of high oscillation contrast over times larger than the excited-state lifetime.

Large-momentum transfer Maintaining a high pulse efficiency over long timescales despite accumulating dephasings and spontaneous emission is particularly interesting in the context of LMT atom interferometry based on sequential π-pulse schemes. So far, the record LMT reported with such schemes, operating on the $^1S_0$–$^3P_1$ transition in ^{87}Sr, is 141 $\hbar k$ [11]. The 21.6 μs excited state lifetime is however a particularly stringent limiting barrier here, and most current efforts with monochromatic pulses focus on delivering shorter pulses, which unfortunately entails large amounts of optical power. Due to their ability to operate on longer coherence times if used in a suitable implementation, polychromatic pulses could permit to overcome this paradigm. We propose here a LMT scheme that fully exploits these benefits [see Fig. 5, top]. It assumes that one arm is put into a dark state—by performing the opening $\pi/2$ pulse on the $^1S_0$–$^3P_0$ clock transition (λ = 698 nm, $\Gamma = 2\pi \times 1$ mHz)—while the other is prepared in the excited state of the $^1S_0$–$^3P_1$ transition—e.g. by using an initial monochromatic pulse—to ensure effective spontaneous emission mitigation. The beamsplitter sequence is then driven by M polychromatic pulses coming from alternate directions: if the pulse duration is set to half the length of the plateaus on Fig. 4, atoms will oscillate between the ground—and excited-state, receiving a momentum $\hbar k$ from each pulse. Light is switched on/off after each pulse to change direction. After M pulses, a LMT of M$\hbar k$ is reached and M further pulses decelerate the addressed arm; after a mirror pulse, the closing sequence is symmetrically constructed to create the interferometer [13].

Compared to the analogous scheme operating on monochromatic pulses only [Fig. 5, bottom], this polychromatic scheme enables a significant LMT improvement. Using typical experimental parameters and a polychromatic field of type (B) with N = 10, we find that the overall interferometer visibility [see Sect. A.2 in the Appendix], which is a good

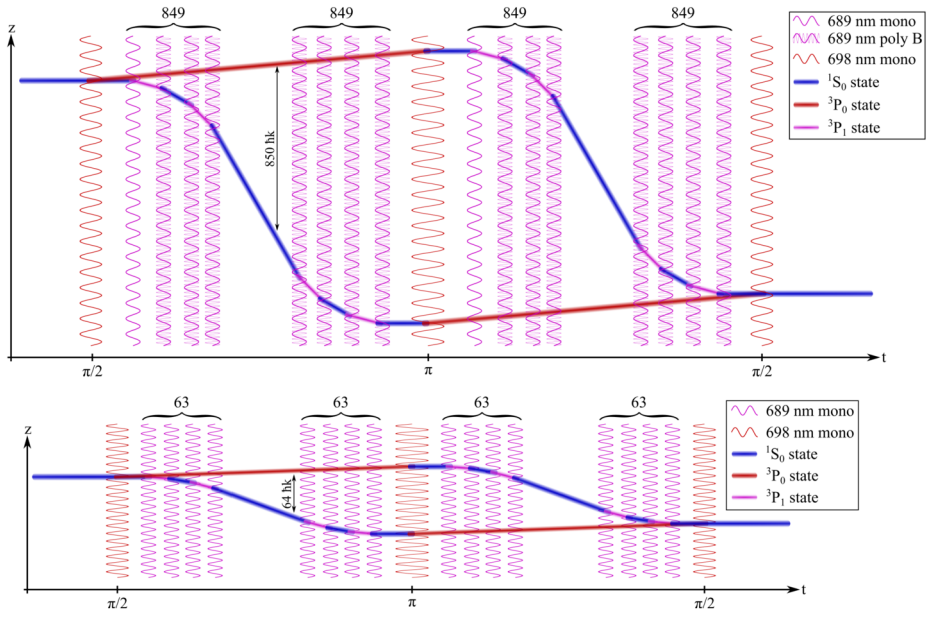

Figure 5 Top: Possible scheme for LMT on ^{87}Sr based on sequential polychromatic π-pulses with spontaneous emission reduction. Bottom: Analogous scheme on ^{87}Sr when operating with monochromatic π-pulses. Due to the benefits of polychromatic pulses, the polychromatic scheme enables a factor of 13 improvement on the momentum separation of the interferometer for the same experimental parameters. The numbers presented here (850 $\hbar k$ and 64 $\hbar k$) correspond to the LMT after which the interferometer visibility drops to 2%, which is obtained from a full calculation of the LMT visibility on both schemes assuming commonly used experimental parameters [see the Appendix, Sect. A.2]

estimate of the expected fringe contrast, drops to 2% after 64 $\hbar k$ in the monochromatic case, versus 850 $\hbar k$ in the polychromatic case [Fig. 9], which corresponds to a factor of 13 improvement in LMT order. Although this polychromatic scheme addresses only one arm of the interferometer (in order for spontaneous emission to be suppressed), it still proves advantageous over a two-arm-based symmetric monochromatic scheme [see Sect. A.1 in the Appendix, Fig. 10], pushing the LMT order achieved (assuming the same 2% visibility threshold) from 151 $\hbar k$ to 850 $\hbar k$, or allowing alternatively an increase of the interferometer visibility at 151 $\hbar k$ from 2% to 55%. This represents a ≈27 times improvement in visibility at no cost of optical power or cooling. We further stress that due to the large polychromatic pulse bandwidth (≈90 MHz), no Doppler-shift compensation is required until ≈3000 $\hbar k$, whereas this would have been necessary to reach LMT beyond ≈600 $\hbar k$ with monochromatic pulses.

We note that we have focused here on demonstrating improvements on the interferometer visibility, yet subtleties may arise as regards the interferometer phase. In particular, the relative uncertainty in the transferred momentum induced by the spectrum extension can result in an uncertainty on the phase and the scale-factor of the interferometer.[8] For instance, as the spectrum bandwidth is several orders of magnitude smaller than light frequencies $\Delta k/k \approx 10^{-8}$, we expect, for an interrogation time $T = 1$ s, the resulting uncertainty on the phase $MkgT^2$ to remain below typical shot noise (1 mrad/shot) up to LMT

[8] Such effects may also be induced by the finite velocity acquired by the atomic cloud, which amounts to its seeing a shifted frequency comb; while the scheme we propose is particularly resilient to frequency detunings as regards pulse efficiencies [see Fig. 3], how this affects the interferometer phase may require a detailed analysis.

orders of $10^4\,\hbar k$. For higher LMT orders, a more careful analysis would be needed to assess these effects and possible trade-offs to be made.

3 Discussion

Compared to other pulse engineering techniques such as composite pulses [5, 16–18], adiabatic passages [19, 20] and Floquet atom optics [22], tailored polychromatic pulses could offer new benefits such as reducing decoherence and the impact of spontaneous emission without requiring any increase of mean laser power. This is achieved, instead, by taking advantage of the non-trivial features of the polychromatic quantum dynamics which allows the circumvention of short pulses. Compared to other works involving polychromatic pulses [24–27, 31], our study is to our knowledge the first to evidence such effect and the first to implement such pulses in a many-atom configuration. Polychromatic pulses are a particular type of shaped pulses, as used for instance in NMR [33], that permit the investigation of optimizing the frequency domain of pulses.

The comb configuration we have proposed offers a versatile and intuitive framework for demonstrating the underlying mechanisms while being convenient to experimentally implement. For a small number of comb teeth, the most direct way would be to use several lasers in parallel at different frequencies and phase lock them; splitting that way the total mean power between a small number of different lasers would already produce visible benefits over the monochromatic case. For higher numbers of field components, which would allow even greater benefits, an option would be to use an electro-optic modulator in a single sideband configuration and generate the requisite spectra with the radio-frequency signal created by an arbitrary waveform generator. While the combs requirements we have identified are commensurate with the current capabilities of commercial modulators, some technical details, such as the precise control of the phase relationship between field components or the robustness of the scheme against imperfections in the design of comb teeth, might need a careful attention.

While we have focused here on comb tailoring in frequency and amplitude, we expect that combining this with comb shaping in phase could allow even greater tailoring options and benefits, which is left for future studies. In particular, while we have focused here on demonstrating improvements on the interferometer visibility, polychromatic pulse shaping in phase could lead to a better control of the interferometer phase. Moreover, the ideas presented here could be extended in the future to arbitrary spectra, such as continuous ones, potentially leading to new findings in the field of pulse frequency spectrum optimization.

4 Conclusions

Polychromatic pulses have the potential to enable the pulse efficiency improvements required to realise next levels of LMT and sensitivity for atom interferometers with no technological push needed on cooling or power, which represents a paradigmatic shift. By mitigating even the most fundamental effects such as spontaneous emission, they enable the use of single-photon transitions with a reduced need to operate on long lifetime clock transitions, opening the route to atom interferometers for fundamental physics [36, 37]. While we have evidenced their benefits on single-photon π-pulses, the idea could be extended to other pulses and multi-photon transitions, having relevance to both current and future fundamental and applied experiments. Furthermore, tailored polychromatic pulses

have the potential to reduce the complexity of atom interferometry systems through enabling high efficiency pulse schemes to be achieved at high temperatures, and through reducing the technological needs of delivering fast, high repetition, pulses. Such technological potential, as well as the robustness against position/velocity shifts, could underpin the development of high-sensitivity robust field-deployable gravity sensors [38, 39]. Moreover, such pulse schemes could be relevant to quantum information approaches that address many atoms, where realising high efficiency and mitigating decoherence are currently major challenges [40].

Appendix

A.1 Single-atom polychromatic dynamics

In this section, we review the properties and give some insight into the dynamics of a single atom subjected to the polychromatic comb models considered in this work. The single-atom dynamics is numerically obtained by solving Eq. (2) [Eq. (1) in the absence of decoherence sources] with some given initial condition. For simplicity, we assume here that the atom is initially in the ground state ($\rho_{gg}(0) = |c_g(0)|^2 = 1$) and we are interested in the excited-state probability ($P_e(t) = |c_e|^2 = \rho_{ee}$) as a function of time. Note that in the specific case of a non-detuned ($\Delta = 0$) atom in the absence of decoherence, the problem becomes fully solvable analytically [41] and we find $P_e(t) = \sin^2 \mathcal{A}(t)/2$ with

$$\mathcal{A}(t) = \int_{-\infty}^{t} \Omega(t')\, dt' = \sum_{n=-N}^{N} \Omega_n \frac{(\sin \delta\omega_n t + \phi_n)}{\delta\omega_n}. \tag{4}$$

For the sake of simplicity, we focus here the analysis on equal amplitude combs (i.e. of type A and B) and assume all field components to be in phase, $\phi_n = 0$.

Assuming first a comb of type B (no resonant component), Fig. 6 shows how adding more and more frequency components modifies the shape of Rabi oscillations. The dynamics [in blue] features a global periodicity, inside which smaller structures appear; these different timescales arise from the two frequency scales of the comb, namely: (i) its spacing $\delta\omega$, which implies a periodicity of $2\pi/\delta\omega$ in the dynamics; (ii) its bandwidth $\approx \mathcal{N}\delta\omega$, which is associated with the shorter timescale of the first maximum, $\tau_{\text{rapid}} \approx \pi/\mathcal{N}\delta\omega$. When N is large enough, flat and extended oscillation plateaus appear, separated by sharp drops as a consequence of the time-dependent Rabi frequency $\Omega(t)$ [plotted in red] being sharply peaked around multiples of $2\pi/\delta\omega$. This behaviour can be qualitatively understood in the time domain where, for a large number of field components, the polychromatic pulse bares similarities with a train of short pulses; in this picture, at $t = 0$, the first pulse of the train would drive a rapid π-pulse arising from all field components being in phase, while all the subsequent pulses, which have a double pulse area, would correspond to quick 2π-pulses (going back and forth the excited-state)—overall producing plateau-shaped Rabi oscillations. While the short term dynamics is therefore similar to a short monochromatic pulse, the later dynamics, such as the existence of plateaus spaced by $\pi/\delta\omega$, is intimately linked to the comb's inner structure. As a consequence, it is advantageous to define the polychromatic π-time as the duration to reach the middle of the first plateau, which is given for a single atom by $\tau_\pi^{\text{poly}} = \pi/\delta\omega$. By setting a polychromatic π-time at this timescale, we are able—at the expense of longer pulses—to exploit the new features of the polychromatic

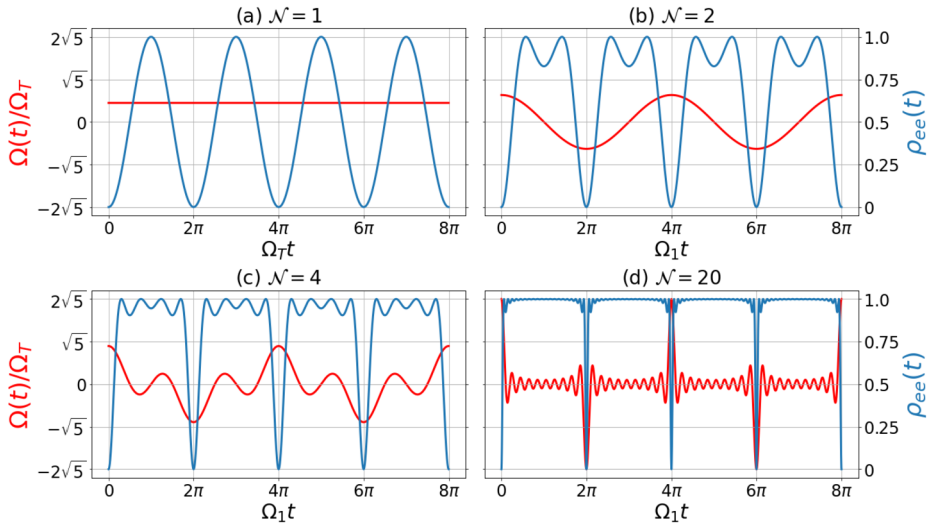

Figure 6 From monochromatic to polychromatic Rabi oscillations—For a comb of type B, plotted is the excited state probability for a single non-detuned ($\Delta = 0$) atom (blue); when gradually increasing the number of peaks at fixed mean power, the standard sinusoidal Rabi oscillations distort to eventually feature extended plateaus. In red, the time-dependent Rabi frequency $\Omega(t)$ corresponding to the considered spectrum. We note that the dynamics displayed here are very general in the sense that changing the total power in the comb would only amount to rescaling the timescale of the dynamics, producing the same curves as a function of $\Omega_1 t$

dynamics, getting additional benefits over short monochromatic pulses, such as an enhanced resilience to spatial inhomogeneities (arising from flat-top Rabi oscillations) and specific comb tailoring options to mitigate contrast loss [see main text].

Figure 7 (right) shows how the dynamics is modified when the comb spacing $\delta\omega$ is changed (as measured here by the comb aspect ration $\epsilon = \delta\omega/\Omega_1$). Not only the periodicity is modified as per $2\pi/\delta\omega$, but also the height of the plateaus is changed. This can be quantified by computing the π-pulse efficiency, which is given by the excited-state probability at mid-plateau time (polychromatic π-time τ_π^{poly}). As visible on Fig. 8, the latter displays a maximum at $\epsilon = 1$, which motivates why such tailoring choice is made in the paper.

For combs of type A (i.e. containing a resonant component), the dynamics also display similar plateaus of length $2\pi/\delta\omega$ [see Fig. 7 (left)]. However, at variance with combs B, the plateaus' length does not correspond to a periodicity in the dynamics: writing the aspect ratio $\epsilon \equiv \delta\omega/\Omega_0 = p/q$, a true global periodicity is only restored after p plateaus, i.e. after a time $2\pi p/\delta\omega = 2\pi q/\Omega_0$. This can be understood from Eq. (4): while all non-resonant terms in the sum oscillate at $\delta\omega$ (hence the overall periodicity for combs B), the resonant component in combs A oscillates at Ω_0. Therefore, the existence of a global periodicity depends on the degree of commensurability between $\delta\omega$ and Ω_0, which is captured through the parameter ϵ. If ϵ is irrational, there is no periodicity in the dynamics, which become quasiperiodic. Interestingly, we observe that the first plateau is very similar to what it is for a comb of type B. As a result, the π-pulse efficiency as a function of comb spacing displays a very similar behaviour than in the case of combs B [see Fig. 8], justifying here as well the choice $\epsilon = 1$ made in this paper.

Finally, we observe [see Fig. 7] that in the limit $\delta\omega \to \infty$ where all non-resonant field component are set to infinity, the dynamics for combs A converges to the expected

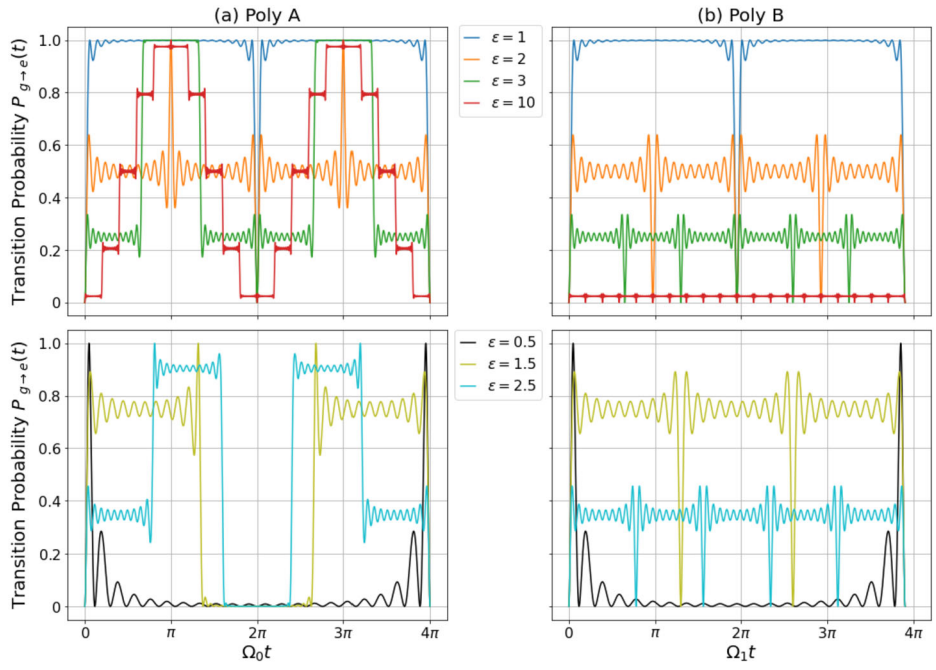

Figure 7 Excited-state probability of a single atom initially prepared in the ground-state and subjected to a polychromatic field with (comb A, left) and without (comb B, right) a resonant component, for different values of the comb aspect ratio ϵ. For combs B, the dynamics display a periodicity of $2\pi/\delta\omega = 2\pi/\epsilon\Omega_1$; for combs A, such segments of length $2\pi/\delta\omega$ do not repeat periodically and it is only if the comb spacing and the resonant component are commensurate, $\epsilon \equiv \delta\omega/\Omega_0 = p/q$ that a global periodicity is restored after $2\pi p/\delta\omega = 2\pi q/\Omega_0$

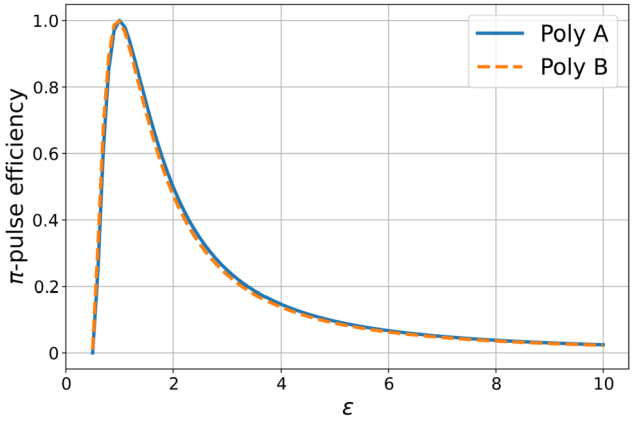

Figure 8 For a non-detuned single atom, π-pulse efficiency as a function of the comb aspect ratio ϵ. The π-pulse efficiency is obtained by taking the transition probability at the polychromatic π-time (middle of the first plateau, given by $\pi/\delta\omega$ in the single-atom case considered here). For combs both with and without a resonant component, the efficiency is maximal at $\epsilon = 1$, which can be seen from Eq. (4). We have used here $N = 10$ pairs of peaks

monochromatic dynamics as the plateaus get smaller and smaller to reconstruct the shape of a Rabi oscillation at frequency Ω_0; in turn, for combs B, the excited-state probability identically converges to zero are there is no resonant component. In the limit, $\delta\omega \to 0$,

the dynamics for both combs A and B converges to rapid monochromatic Rabi oscillations at the total Rabi frequency Ω_T, as all field components coalesce.

A.2 Large-momentum transfer and interferometer visibility

We consider here the two LMT schemes (resp. polychromatic and monochromatic) depicted on Fig. 5 as well as the monochromatic symmetric scheme depicted on Fig. 10 and assume the following commonly-used parameters: $T = 3\ \mu$K, $\sigma_{\text{pos}} = 160\ \mu$m, $\sigma_{\text{beam}} = 0.75$ mm, $P = 40$ mW (which correspond to $\tau_\pi^{\text{mono}} = 161$ ns). We assume the polychromatic field to be of type (B) with 10 pairs of peaks (yielding $\tau_\pi^{\text{poly}} = 720$ ns). Figure 9 compares the interferometer visibility of these three LMT sequences as a function of LMT order. It is defined here as the product of the individual efficiencies of all the pulses involved in the sequence, taking into account cloud averaging and decoherence mechanisms described previously as well as cloud expansion along the sequence. We have checked on shorter pulse sequences that compared to an exact simulation of the full interferometric sequence, this common approximation of multiplying individual pulse efficiencies yields very similar results at reduced computational cost, with a tendency to only slightly underestimate the overall interferometer visibility. No Doppler-shift compensation is required here due to the large polychromatic pulse bandwidth (≈90 MHz) which corresponds to ≈3000 $\hbar k$.[9] We assume here no time delay between pulses. Possible light shift effects are expected to be comparable to the monochromatic case as the light shift experienced by a given atom is dominated by the closest-resonant peak(s); details of these may result in additional tailoring of the field, which will be the object of follow-up studies. We find that the overall interferometer visibility drops to 2% after 64 $\hbar k$ in the simple monochro-

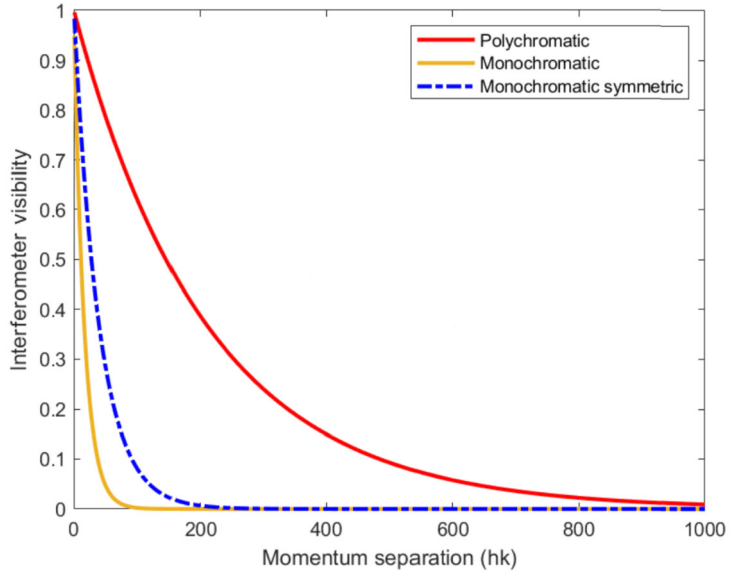

Figure 9 Interferometer visibility of the polychromatic (red), monochromatic (yellow) and monochromatic symmetric (blue) LMT sequences respectively depicted on Fig. 5 (top, bottom) and Fig. 10. We have used here the same parameters: $\sigma_{\text{pos}} = 160\ \mu$m, $\sigma_{\text{beam}} = 0.75$ mm $T = 3\ \mu$K and a laser power of 40 mW. The polychromatic sequence uses comb B with $N = 10$ and $\epsilon = 1$. We assume here no time delay between pulses

[9] For the monochromatic case, this also holds up to 600 $\hbar k$.

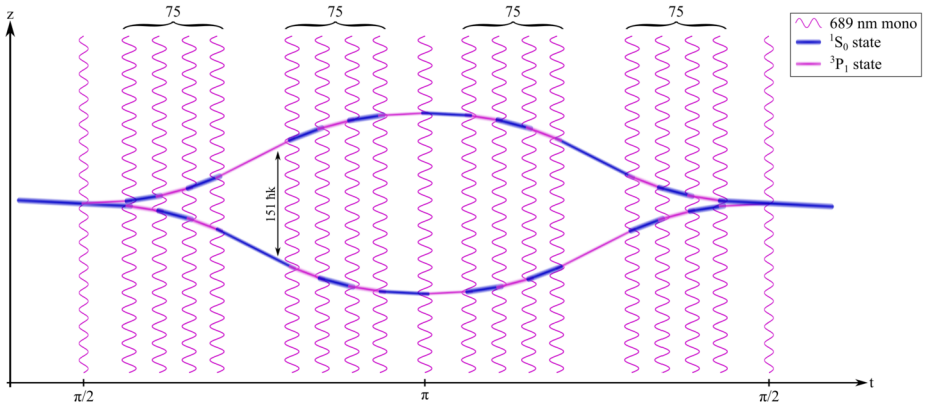

Figure 10 Monochromatic symmetric LMT scheme. Due to the large pulse bandwidth (≈19 MHz), if no arm is put into a dark state and no particular Doppler shift compensation is applied, each pulse will act on both arms of the interferometer with good efficiency and impart $2\hbar k$ of momentum splitting—resulting in a symmetric scheme

matic case and $151\,\hbar k$ in the monochromatic symmetric configuration, versus $850\,\hbar k$ in the polychromatic case.

Acknowledgements
We thank Andrew Lamb, David Sedlak and Yu-Hung Lien for discussions.

Funding
We acknowledge funding from the Engineering and Physical Sciences Research Council (EP/T001046/1) and Innovate UK (104613) as part of the UK National Quantum Technologies Programme, and from the Science and Technology Facilities Council (ST/T006536/1).

Abbreviations
Not applicable.

Availability of data and materials
The authors declare that all data supporting the findings of this study are available within this article and Supplementary Material. It can be available from the corresponding author upon reasonable request. The code that supports the findings of this study can be available from the corresponding author upon reasonable request.

Declarations

Ethics approval and consent to participate
Not applicable.

Competing interests
The authors declare no competing interests.

Author contributions
S.L. conceived the idea and the scheme. S.L., O.E and R.H. derived the theoretical framework and code, and performed the calculations. S.L., M.L. and M.H. contributed throughout and supervised the research. All authors contributed to reviewing and assessing the results, and to the development and review of the manuscript. O.E. and R.H. contributed equally to this work.

Authors' information
Not applicable.

Publisher's Note

Received: 29 September 2022 Accepted: 11 February 2023 Published online: 08 March 2023

References

1. Berman P. Atom interferometry. 1st ed. San Diego: Academic Press; 1997.
2. Kasevich M, Chu S. Atomic interferometry using stimulated Raman transitions. Phys Rev Lett. 1991;67(2):181–4. https://doi.org/10.1103/physrevlett.67.181.
3. Giltner D, McGowan R, Lee S. Atom interferometer based on Bragg scattering from standing light waves. Phys Rev Lett. 1995;75(14):2638–41. https://doi.org/10.1103/physrevlett.75.2638.
4. Rabi II. Space quantization in a gyrating magnetic field. Phys Rev. 1937;51(8):652–4. https://doi.org/10.1103/physrev.51.652.
5. Dunning A, Gregory R, Bateman J, Cooper N, Himsworth M, Jones JA, Freegarde T. Composite pulses for interferometry in a thermal cold atom cloud. Phys Rev A. 2014;90:033608. https://doi.org/10.1103/PhysRevA.90.033608.
6. Szigeti SS, Debs JE, Hope JJ, Robins NP, Close JD. Why momentum width matters for atom interferometry with Bragg pulses. New J Phys. 2012;14(2):023009. https://doi.org/10.1088/1367-2630/14/2/023009.
7. Butts DL, Kotru K, Kinast JM, Radojevic AM, Timmons BP, Stoner RE. Efficient broadband Raman pulses for large-area atom interferometry. J Opt Soc Am B. 2013;30(4):922–7. https://doi.org/10.1364/JOSAB.30.000922.
8. McGuirk JM, Snadden MJ, Kasevich MA. Large area light-pulse atom interferometry. Phys Rev Lett. 2000;85(21):4498–501. https://doi.org/10.1103/physrevlett.85.4498.
9. McDonald GD, Kuhn CCN, Bennetts S, Debs JE, Hardman KS, Close JD, Robins NP. A faster scaling in acceleration-sensitive atom interferometers. Europhys Lett. 2014;105(6):63001. https://doi.org/10.1209/0295-5075/105/63001.
10. Chiow S, Kovachy T, Chien H, Kasevich M. 102 $\hbar k$ large area atom interferometers. Phys Rev Lett. 2011;107(13):130403. https://doi.org/10.1103/physrevlett.107.130403.
11. Rudolph J, Wilkason T, Nantel M, Swan H, Holland CM, Jiang Y, Garber BE, Carman SP, Hogan JM. Large momentum transfer clock atom interferometry on the 689 nm intercombination line of strontium. Phys Rev Lett. 2020;124:083604. https://doi.org/10.1103/PhysRevLett.124.083604.
12. Graham PW, Hogan JM, Kasevich MA, Rajendran S, Romani RW. Mid-band gravitational wave detection with precision atomic sensors. arXiv preprint. 2017. arXiv:1711.02225.
13. McDonald GD, Kuhn CCN, Bennetts S, Debs JE, Hardman KS, Johnsson M, Close JD, Robins NP. 80 $\hbar k$ momentum separation with Bloch oscillations in an optically guided atom interferometer. Phys Rev A. 2013;88:053620. https://doi.org/10.1103/PhysRevA.88.053620.
14. Mazzoni T, Zhang X, Del Aguila R, Salvi L, Poli N, Tino GM. Large-momentum-transfer Bragg interferometer with strontium atoms. Phys Rev A. 2015;92:053619. https://doi.org/10.1103/PhysRevA.92.053619.
15. Gebbe M, Siemß J-N, Gersemann M, Müntinga H, Herrmann S, Lämmerzahl C, Ahlers H, Gaaloul N, Schubert C, Hammerer C, Abend S, Rasel E. Twin-lattice atom interferometry. Nat Commun. 2021;12(1):2544. https://doi.org/10.1038/s41467-021-22823-8.
16. Berg P, Abend S, Tackmann G, Schubert C, Giese E, Schleich WP, Narducci FA, Ertmer W, Rasel EM. Composite-light-pulse technique for high-precision atom interferometry. Phys Rev Lett. 2015;114:063002. https://doi.org/10.1103/PhysRevLett.114.063002.
17. Saywell J, Kuprov I, Goodwin D, Carey M, Freegarde T. Optimal control of mirror pulses for cold-atom interferometry. Phys Rev A. 2018;98(2):023625. https://doi.org/10.1103/physreva.98.023625.
18. Levitt M, Freeman R. Compensation for pulse imperfections in NMR spin-echo experiments. J Magn Reson. 1981;43(1):65–80. https://doi.org/10.1016/0022-2364(81)90082-2.
19. Weitz M, Young B, Chu S. Atomic interferometer based on adiabatic population transfer. Phys Rev Lett. 1994;73:2563–6. https://doi.org/10.1103/PhysRevLett.73.2563.
20. Kotru K, Butts DL, Kinast JM, Stoner RE. Large-area atom interferometry with frequency-swept Raman adiabatic passage. Phys Rev Lett. 2015;115(10):103001. https://doi.org/10.1103/physrevlett.115.103001.
21. Solaro C, Debavelaere C, Cladé P, Guellati-Khelifa S. Atom interferometer driven by a picosecond frequency comb. Phys Rev Lett. 2022;129(17):173204. https://doi.org/10.1103/physrevlett.129.173204.
22. Wilkason T, Nantel M, Rudolph J, Jiang Y, Garber BE, Swan H, Carman SP, Abe M, Hogan JM. Atom interferometry with floquet atom optics. Phys Rev Lett. 2022;129(18):183202. https://doi.org/10.1103/PhysRevLett.129.183202.
23. Allen L, EberlyJH. Optical resonance and two-level atoms. New York: Dover; 1997.
24. Chakmakjian S, Koch K, Stroud C. Observation of resonances at subharmonics of the Rabi frequency in the saturated absorption of a 100% amplitude-modulated laser beam. J Opt Soc Am B. 1988;5(10):2015–20. https://doi.org/10.1364/JOSAB.5.002015.
25. Ruyten WM. Harmonic behavior of the multiple quantum resonances of a two-level atom driven by a fully-amplitude-modulated field. Phys Rev A. 1989;40:1447–55. https://doi.org/10.1103/PhysRevA.40.1447.
26. Lam P, Savage CM. Complete atomic population inversion using correlated sidebands. Phys Rev A. 1994;50:3500–4. https://doi.org/10.1103/PhysRevA.50.3500.
27. Li DX, Shao XQ. Rapid population transfer of a two-level system by a polychromatic driving field. Sci Rep. 2019;9(1):9023. https://doi.org/10.1038/s41598-019-45558-5.
28. Wang J, Zhu Y, Jiang KJ, Zhan MS. Bichromatic electromagnetically induced transparency in cold rubidium atoms. Phys Rev A. 2003;68:063810. https://doi.org/10.1103/PhysRevA.68.063810.
29. Manson N, Wei C, Martin J. Response of a two-level system driven by two strong fields. Phys Rev Lett. 1996;76:3943–6. https://doi.org/10.1103/PhysRevLett.76.3943.
30. Freedhoff H, Chen Z. Resonance fluorescence of a two-level atom in a strong bichromatic field. Phys Rev A. 1990;41:6013–22. https://doi.org/10.1103/PhysRevA.41.6013.
31. Ficek Z, Seke J, Soldatov AV, Adam G. Fluorescence spectrum of a two-level atom driven by a multiple modulated field. Phys Rev A. 2001;64:013813. https://doi.org/10.1103/PhysRevA.64.013813.
32. Hu L, Poli N, Salvi L, Tino GM. Atom interferometry with the sr optical clock transition. Phys Rev Lett. 2017;119:263601. https://doi.org/10.1103/PhysRevLett.119.263601.
33. Vandersypen LMK, Chuang IL. NMR techniques for quantum control and computation. Rev Mod Phys. 2005;76(4):1037–69. https://doi.org/10.1103/revmodphys.76.1037.

34. Luo Y, Yan S, Hu Q, Jia A, Wei C, Yang J. Contrast enhancement via shaped Raman pulses for thermal cold atom cloud interferometry. Eur Phys J D. 2016;70(12):262. https://doi.org/10.1140/epjd/e2016-70428-6.
35. Fang B, Mielec N, Savoie D, Altorio M, Landragin A, Geiger R. Improving the phase response of an atom interferometer by means of temporal pulse shaping. New J Phys. 2018;20(2):023020. https://doi.org/10.1088/1367-2630/aaa37c.
36. Graham P, Hogan J, Kasevich M, Rajendran S. New method for gravitational wave detection with atomic sensors. Phys Rev Lett. 2013;110(17):171102. https://doi.org/10.1103/physrevlett.110.171102.
37. Badurina L, Bentine E, Blas D, Bongs K, Bortoletto D, Bowcock T, Bridges K, Bowden W, Buchmueller O, Burrage C, Coleman J, Elertas G, Ellis J, Foot C, Gibson V, Haehnelt MG, Harte T, Hedges S, Hobson R, Holynski M, Jones T, Langlois M, Lellouch S, Lewicki M, Maiolino R, Majewski P, Malik S, March-Russell J, McCabe C, Newbold D, Sauer B, Schneider U, Shipsey I, Singh Y, Uchida MA, Valenzuela T, van der Grinten M, Vaskonen V, Vossebeld J, Weatherill D, Wilmut I. AION: an atom interferometer observatory and network. J Cosmol Astropart Phys. 2020;2020(5):011.
38. Ménoret V, Vermeulen P, Moigne NL, Bonvalot S, Bouyer P, Landragin A, Desruelle B. Gravity measurements below 10^{-9} g with a transportable absolute quantum gravimeter. Sci Rep. 2018;8(1):12300. https://doi.org/10.1038/s41598-018-30608-1.
39. Stray B, Lamb A, Kaushik A, Vovrosh J, Rodgers A, Winch J, Hayati F, Boddice D, Stabrawa A, Niggebaum A, Langlois M, Lien Y-H, Lellouch S, Roshanmanesh S, Ridley K, de Villiers G, Brown G, Cross T, Tuckwell G, Faramarzi A, Metje N, Bongs K, Holynski M. Quantum sensing for gravity cartography. Nature. 2022;602(7898):590–4. https://doi.org/10.1038/s41586-021-04315-3.
40. Saffman M. Quantum computing with atomic qubits and Rydberg interactions: progress and challenges. J Phys, B At Mol Opt Phys. 2016;49(20):202001. https://doi.org/10.1088/0953-4075/49/20/202001.
41. Shore BW. Manipulating quantum structures using laser pulses. Cambridge: Cambridge University Press; 2011. https://doi.org/10.1017/CBO9780511675713.